J|A|C|S ARTICLES

Published on Web 05/18/2010

What Factors Influence the Rate Constant of Substrate Epoxidation by Compound I of Cytochrome P450 and Analogous Iron(IV)-Oxo Oxidants?

Devesh Kumar,*[,†] Baharan Karamzadeh,[‡] G. Narahari Sastry,[†] and Sam P. de Visser*[,‡]

Molecular Modelling Group, Indian Institute of Chemical Technology, Hyderabad 500-607, India, and The Manchester Interdisciplinary Biocenter and the School of Chemical Engineering and Analytical Science, The University of Manchester, 131 Princess Street, Manchester M1 7DN, United Kingdom

Received December 16, 2009; E-mail: sam.devisser@manchester.ac.uk; dkclcre@yahoo.com

Abstract: The cytochromes P450 are a versatile range of mono-oxygenase enzymes that catalyze a variety of different chemical reactions, of which the key reactions include aliphatic hydroxylation and C=C double bond epoxidation. To establish the fundamental factors that govern substrate epoxidation by these enzymes we have done a systematic density functional theory study on substrate epoxidation by the active species of P450 enzymes, namely the iron(IV)-oxo porphyrin cation radical oxidant or Compound I. We show here, for the first time, that the rate constant of substrate epoxidation, and hence the activation energy, correlates with the ionization potential of the substrate as well as with intrinsic electronic properties of the active oxidant such as the polarizability volume. To explain these findings we present an electron-transfer model for the reaction mechanism that explains the factors that determine the barrier heights and developed a valence bond (VB) curve crossing mechanism to rationalize the observed trends. In addition, we have found a correlation for substrate epoxidation reactions catalyzed by a range of heme and nonheme iron(IV)-oxo oxidants with the strength of the O−H bond in the iron-hydroxo complex, i.e. BDE_{OH}, which is supported by the VB model. Finally, the fundamental factors that determine the regioselectivity change between substrate hydroxylation and epoxidation are discussed. It is shown that the regioselectivity of aliphatic hydroxylation versus double bond epoxidation is not influenced by the choice of the oxidant but is purely substrate dependent.

Introduction

The cytochromes P450 (P450s) are important heme based mono-oxygenases that take part in key biomolecular processes in the body that include detoxification processes in the liver, the biosynthesis of hormones, and metabolism of drugs.[1] The P450s bind molecular oxygen on a heme center and transfer one of its oxygen atoms to a substrate, while the second oxygen atom originating from O_2 is reduced to a water molecule. A versatile range of oxygen atom transfer reactions is catalyzed by the P450s that consists of aliphatic and aromatic hydroxylation, heteroatom oxidation, and double bond epoxidation.[2] For instance, unsaturated fatty acids are epoxidized by bacterial as well as human liver P450 enzymes.[3] Thus, the biosynthesis of hormones in cockroaches involves the epoxidation of methyl farnesoate, a reaction that is catalyzed by P450 15A1.[4] The fundamental factors that determine the mechanism and kinetics of substrate epoxidation by P450 enzymes are currently unknown. To gain insight into the factors that govern the epoxidation process, we present a systematic study on double bond epoxidation mechanisms by metal-oxo oxidants such as those that appear in P450 enzymes for the first time and investigate the intrinsic features of substrate and oxidant that determine the reaction kinetics.

The active site of P450 enzymes is a heme group that is linked to the protein via a thiolate bridge of a cysteinate residue of the protein. Figure 1 shows the active site of a well-studied P450 enzyme, namely $P450_{cam}$.[5] P450 enzymes undergo a complicated catalytic cycle that starts from the resting state where a water molecule fills the sixth binding site of iron. Upon substrate entrance into the binding pocket, this water molecule is displaced; the heme is reduced and binds molecular oxygen.

[†] Indian Institute of Chemical Technology.
[‡] The University of Manchester.

(1) (a) Sono, M.; Roach, M. P.; Coulter, E. D.; Dawson, J. H. *Chem. Rev.* **1996**, *96*, 2841–2888. (b) Kadish, K. M.; Smith, K. M.; Guilard, R., Eds. *The Porphyrin Handbook*; Academic Press: San Diego, CA, 2000; Vol. 4. (c) Guengerich, F. P. *Chem. Res. Toxicol.* **2001**, *14*, 611–650. (d) Groves, J. T. *Proc. Natl. Acad. Sci. U.S.A.* **2003**, *100*, 3569–3574. (e) Ortiz de Montellano, P. R., Ed. *Cytochrome P450: Structure, Mechanism and Biochemistry*, 3rd ed.; Kluwer Academic/Plenum Publishers: New York, 2004. (f) Munro, A. W.; Girvan, H. M.; McLean, K. J. *Nat. Prod. Rep.* **2007**, *24*, 585–609.

(2) (a) Groves, J. T. Models and Mechanisms of Cytochrome P450 Action. In *Cytochrome P450: Structure, Mechanism and Biochemistry*, 3rd ed.; Ortiz de Montellano, P. R., Ed.; Kluwer Academic/Plenum Publishers: New York, 2005; Chapter 1, pp 1−44. (b) Nam, W. *Acc. Chem. Res.* **2007**, *40*, 522–531. (c) Nam, W. In *Comprehensive Coordination Chemistry II*; Que, L., Jr., Tolman, W. B., Eds.; Elsevier Ltd.: New York, 2004; Vol. 8, pp 281−307.

(3) (a) Daikh, B. E.; Lasker, J. M.; Raucy, J. L.; Koop, D. R. *J. Pharmacol. Exp. Therap.* **1994**, *271*, 1427–1433. (b) Çelik, A.; Sperandio, D.; Speight, R. E.; Turner, N. J. *Org. Biomol. Chem.* **2005**, *3*, 2688–2690.

 10.1021/ja9106176

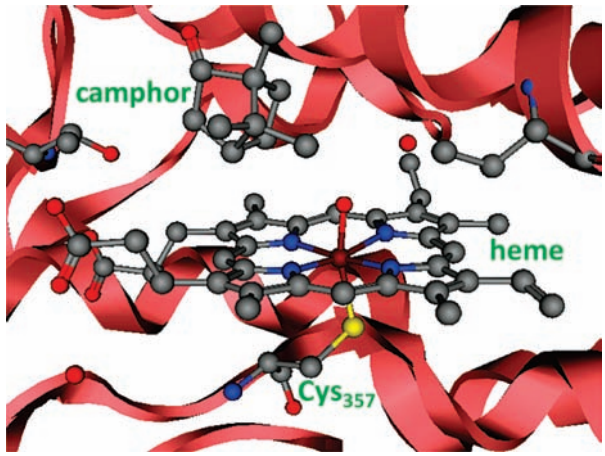

Figure 1. Active site of $P450_{cam}$ as taken from the 1DZ9 pdb file[3] with residues labeled as in the pdb file.

Thereafter, a second reduction followed by two protonation steps gives an iron(IV)-oxo heme cation radical species that is also known as Compound I (Cpd I). This species reacts with substrates via oxygen atom transfer to give oxygenated products. Indirect evidence of Cpd I through kinetic isotope effects and product distributions has implicated it to be the key oxidant involved in mono-oxygenase reactions with substrates.[6] More recent low pressure mass spectrometric studies[7] on biomimetic iron-porphyrins and computational modeling[8] have shown it to be a very efficient oxidant of substrate hydroxylation and epoxidation reactions.

Iron(IV)-oxo oxidants are the active species of mononuclear heme as well as nonheme iron containing enzymes, and recently spectroscopic evidence of the iron(IV)-oxo species of the nonheme enzymes of taurine/α-ketoglutarate dioxygenase (TauD), prolyl-4-hydroxylase, and α-ketoglutarate dependent halogenase was found.[9] In addition, several biomimetic nonheme iron(IV)-oxo species were detected and characterized with a range of spectroscopic techniques.[10] These biomimetic oxidants have been shown to react with substrates via aliphatic hydroxylation as well as epoxidation reactions very efficiently. The key features that influence the epoxidation mechanism and kinetics are unknown as well as what determines the regioselectivity of aliphatic hydroxylation versus epoxidation.

Substrate epoxidation by P450 enzymes has been extensively studied.[11] For instance, palmitoleic acid and related monounsaturated fatty acids were found to be oxidized by P450 enzymes to hydroxylated and epoxidized products.[12] These studies implicated a common oxidant for the reaction products, presumably an iron(IV)-oxo heme cation radical species such as Cpd I. $P450_{cam}$ studies using *cis*-β-methyl styrene as a substrate gave strong enantioselectivity with an 89:11 preference of the 1*S*,2*R* epoxide product over the 1*R*,2*S* form.[13] Molecular dynamics docking calculations predicted the substrate binding orientation to be responsible for this product ratio. Several studies reported epoxidation of non-natural substrates, such as propene, styrene, and cyclohexene.[14] Interestingly, the kinetics of styrene epoxidation by two P450 isozymes, CYP119 and CYP102HD, was found to be very similar,[14d] and so was the kinetics of aliphatic hydroxylation of benzyl alcohol by these isozymes. The regioselectivity of substrate hydroxylation versus epoxidation was investigated with two P450 isozymes and two of its mutants using cyclohexene and *cis*- and *trans*-2-butene as substrates.[15] The results on cyclohexene gave a relatively constant alcohol versus epoxide product ratio between 1.0 and 2.4, whereas with the other substrates large differences in the product ratios were observed.

Substrate epoxidation by biomimetic iron−porphyrin complexes has been extensively studied over the past 30 years.[16,17] For instance, it was shown that the axial ligand *trans* to the oxo group in biomimetic Cpd I complexes affects the oxidative power of the active species that correlated with the rate constant of styrene epoxidation.[18] More recent studies of Nam et al.[19] also showed an axial ligand effect for aliphatic hydroxylation and phosphorylation reactions by nonheme iron(IV)-oxo species. In the case of aliphatic hydroxylation reactions by metal-oxo oxidants Mayer et al. showed that the rate constant of hydrogen atom abstraction is related to the energy required to break the

(4) Helvig, C.; Koener, J. F.; Unnithan, G. C.; Feyereisen, R. *Proc. Natl. Acad. Sci. U.S.A.* **2004**, *101*, 4024–4029.
(5) Schlichting, I.; Berendzen, J.; Chu, K.; Stock, A. M.; Maves, S. A.; Benson, D. E.; Sweet, R. M.; Ringe, D.; Petsko, G. A.; Sligar, S. G. *Science* **2000**, *287*, 1615–1622.
(6) (a) Egawa, T.; Shimada, H.; Ishimura, Y. *Biochem. Biophys. Res. Commun.* **1994**, *201*, 1464–1469. (b) Kellner, D. G.; Hung, S.-C.; Weiss, K. E.; Sligar, S. G. *J. Biol. Chem.* **2002**, *277*, 9641–9644.
(7) (a) Chiavarino, B.; Cipollini, R.; Crestoni, M. E.; Fornarini, S.; Lanucara, F.; Lapi, A. *J. Am. Chem. Soc.* **2008**, *130*, 3208–3217. (b) Crestoni, M. E.; Fornarini, S.; Lanucara, F. *Chem.—Eur. J.* **2009**, *15*, 7863–7866.
(8) (a) Meunier, B.; de Visser, S. P.; Shaik, S. *Chem. Rev.* **2004**, *104*, 3947–3980. (b) Shaik, S.; Kumar, D.; de Visser, S. P.; Altun, A.; Thiel, W. *Chem. Rev.* **2005**, *105*, 2279–2328. (c) Shaik, S.; Cohen, S.; Wang, Y.; Chen, H.; Kumar, D.; Thiel, W. *Chem. Rev.* **2010**, *110*, 949–1017.
(9) (a) Proshlyakov, D. A.; Henshaw, T. F.; Monterosso, G. R.; Ryle, M. J.; Hausinger, R. P. *J. Am. Chem. Soc.* **2004**, *126*, 1022–1023. (b) Riggs-Gelasco, P. J.; Price, J. C.; Guyer, R. B.; Brehm, J. H.; Barr, E. W.; Bollinger, J. M., Jr.; Krebs, C. *J. Am. Chem. Soc.* **2004**, *126*, 8108–8109. (c) Hoffart, L. M.; Barr, E. W.; Guyer, R. B.; Bollinger, J. M., Jr.; Krebs, C. *Proc. Natl. Acad. Sci. U.S.A.* **2006**, *103*, 14738–14743. (d) Galonić, D. P.; Barr, E. W.; Walsh, C. T.; Bollinger, J. M., Jr.; Krebs, C. *Nat. Chem. Biol.* **2007**, *3*, 113–116.
(10) For example, see: (a) Rohde, J.-U.; In, J.-H.; Lim, M. H.; Brennessel, W. W.; Bukowski, M. R.; Stubna, A.; Münck, E.; Nam, W.; Que, L., Jr. *Science* **2003**, *299*, 1037–1039. (b) Bukowski, M. R.; Koehntop, K. D.; Stubna, A.; Bominaar, E. L.; Halfen, J. A.; Münck, E.; Nam, W.; Que, L., Jr. *Science* **2005**, *310*, 1000–1002. (c) Jensen, M. P.; Costas, M.; Ho, R. Y. N.; Kaizer, J.; Mairate i Payeras, A.; Münck, E.; Que, L., Jr.; Rohde, J.-U.; Stubna, A. *J. Am. Chem. Soc.* **2005**, *127*, 10512–10525. (d) De Oliveira, F. T.; Chanda, A.; Banerjee, D.; Shan, X.; Mondal, S.; Que, L., Jr.; Bominaar, E. L.; Münck, E.; Collins, T. J. *Science* **2007**, *315*, 835–838.
(11) (a) Guengerich, F. P. *Arch. Biochem. Biophys.* **2003**, *409*, 59–71. (b) McLean, K. J.; Munro, A. W. *Drug Metabol. Rev.* **2008**, *40*, 427–446.
(12) Ruettinger, R. T.; Fulco, A. J. *J. Biol. Chem.* **1981**, *256*, 5728–5734.
(13) Ortiz de Montellano, P. R.; Fruetel, J. A.; Collins, J. R.; Camper, D. L.; Loew, G. H. *J. Am. Chem. Soc.* **1991**, *113*, 3195–3196.
(14) (a) Groves, J. T.; Avaria-Neisser, G. E.; Fish, K. M.; Imachi, M.; Kuczkowski, R. L. *J. Am. Chem. Soc.* **1986**, *108*, 3837–3838. (b) Alcalde, M.; Farinas, E. T.; Arnold, F. H. *J. Biomol. Screen.* **2004**, *9*, 141–146. (c) Dansette, P. M.; Bertho, G.; Mansuy, D. *Biochem. Biophys. Res. Commun.* **2005**, *338*, 450–455. (d) Yuan, X.; Wang, Q.; Horner, J. H.; Sheng, X.; Newcomb, M. *Biochemistry* **2009**, *48*, 9140–9146.
(15) Vaz, A. D. N.; McGinnity, D. F.; Coon, M. J. *Proc. Natl. Acad. Sci. U.S.A.* **1998**, *95*, 3555–3560.
(16) For example, see: (a) Groves, J. T.; Subramanian, D. V. *J. Am. Chem. Soc.* **1984**, *106*, 2177–2181. (b) Solomon, E. I.; Brunold, T. C.; Davis, M. I.; Kemsley, J. N.; Lee, S.-K.; Lehnert, N.; Neese, F.; Skulan, A. J.; Yang, Y.-S.; Zhou, J. *Chem. Rev.* **2000**, *100*, 235–349. (c) Costas, M.; Mehn, M. P.; Jensen, M. P.; Que, L., Jr. *Chem. Rev* **2004**, *104*, 939–986. (d) Bruijnincx, P. C. A.; van Koten, G.; Klein Gebbink, R. J. M. *Chem. Soc. Rev.* **2008**, *37*, 2716–2744.

C−H bond, i.e. BDE_{CH}, as defined by eq 1.[20] This relationship was later found for substrate hydroxylation by a range of different iron- and manganese-oxo oxidants.[21]

$$SubH \rightarrow Sub^{\cdot} + H^{\cdot} + BDE_{CH} \quad (1)$$

In contrast to this, no correlations are known that relate the rate constant of substrate epoxidation by metal-oxo complexes as a function of substrate and/or oxidant properties. To understand the regioselectivity difference of substrate epoxidation versus hydroxylation, it is important to characterize the fundamental factors that determine the rate constant and hence the free energy of activation of substrate epoxidation and hydroxylation by metal-oxo oxidants. That will enable one to predict barrier heights and rate constants from empirical values. Currently, very little is known on the factors that influence the rate constant of substrate epoxidation and no systematic studies have been reported yet. Therefore, in this work we present models that link a range of substrate epoxidation reactions by metal-oxo oxidants with intrinsic chemical and physical properties of the reactants. In principle, substrate epoxidation requires the conversion of a double bond of an olefin into a single bond concomitant with the abstraction of an oxygen atom to bridge this bond. As will be seen in this work, the energy of the π-bond of the olefin is correlated to the ionization potential of the substrate, which subsequently relates to the barrier height of an epoxidation reaction. Using thermodynamic cycles and a valence bond curve crossing diagram, we generalize substrate epoxidation by iron(IV)-oxo oxidants and explain what the electronic factors are that determine the reactivity patterns. Thus, we explain the fundamental differences of substrate epoxidation versus aliphatic hydroxylation based on the electronic properties of the individual reactants, substrate, and oxidant. The studies show what intrinsic electronic properties of the substrate determine the regioselectivity of epoxidation over hydroxylation.

Methods

The calculations described in this work utilize density functional theory (DFT) as implemented in the *Jaguar* 7.6 and *Gaussian*-03 program packages.[22,23] All geometries were fully optimized (without any constraints) in *Jaguar* followed by an analytical frequency in *Gaussian*. Local minima had real frequencies only, whereas transition state structures were characterized by a single imaginary frequency that corresponds to the appropriate mode. All calculations reported here were performed with the B3LYP hybrid density functional method,[24] since this method is capable of reproducing free energies of activation of substrate epoxidation and hydroxylation reactions by iron(IV)-oxo complexes within ~3 kcal mol^{-1} with respect to experiment.[25] Recent studies of a series of hydrogen abstraction reactions by P450 enzyme models showed[26,27] that this is a systematic error and a linear correlation with the bond dissociation energy of the C−H bond of the substrate was found with a standard deviation of ~1 kcal mol^{-1}. Furthermore, these computational methods were shown to accurately reproduce experimentally determined kinetic isotope effects,[28] electron paramagnetic resonance parameters,[29] and vibrational spectra.[30] The methods, therefore, should be suitable for calculations on trends in substrate epoxidation mechanisms as well. Extensive test calculations with alternative density functional methods predicted trends similar to those obtained with B3LYP.[31]

Geometry optimizations and frequency calculations were performed with a double-ζ quality LACVP basis set on iron (including an Effective Core Potential) coupled to 6-31G on the remaining atoms, basis set B1.[32] Subsequently, single-point calculations were performed in *Jaguar* utilizing a triple-ζ quality LACV3P+ basis

(17) For example, see: (a) Groves, J. T.; Myers, R. S. *J. Am. Chem. Soc.* **1983**, *105*, 5791–5796. (b) Groves, J. T.; Watanabe, Y. *J. Am. Chem. Soc.* **1986**, *108*, 507–508. (c) Collman, J. P.; Kodadek, T.; Brauman, J. I. *J. Am. Chem. Soc.* **1986**, *108*, 2588–2594. (d) Ostović, D.; Bruice, T. C. *J. Am. Chem. Soc.* **1989**, *111*, 6511–6517. (e) Collman, J. P.; Brauman, J. I.; Hampton, P. D.; Tanaka, H.; Bohle, D. S.; Hembre, R. T. *J. Am. Chem. Soc.* **1990**, *112*, 7980–7984. (f) Groves, J. T.; Gross, Z.; Stern, M. K. *Inorg. Chem.* **1994**, *33*, 5065–5072. (g) Nam, W.; Lim, M. H.; Lee, H. J.; Kim, C. *J. Am. Chem. Soc.* **2000**, *122*, 6641–6647. (h) Stephenson, N. A.; Bell, A. T. *Inorg. Chem.* **2006**, *45*, 2758–2766. (i) Collman, J. P.; Zeng, L.; Wang, H. J. H.; Lei, A.; Brauman, J. I. *Eur. J. Org. Chem.* **2006**, 2707–2714. (j) Song, W. J.; Sun, Y. J.; Choi, S. K.; Nam, W. *Chem.—Eur. J.* **2006**, *12*, 130–137. (k) Song, W. J.; Seo, M. S.; DeBeer George, S.; Ohta, T.; Song, R.; Kang, M.-J.; Tosha, T.; Kitagawa, T.; Solomon, E. I.; Nam, W. *J. Am. Chem. Soc.* **2007**, *129*, 1268–1277. (l) Hessenauer-Ilicheva, N.; Franke, A.; Meyer, D.; Woggon, W.-D.; van Eldik, R. *J. Am. Chem. Soc.* **2007**, *129*, 12473–12479. (m) Hull, J. F.; Sauer, E. L. O.; Incarvito, C. D.; Faller, J. W.; Brudvig, G. W.; Crabtree, R. H. *Inorg. Chem.* **2009**, *48*, 488–495. (n) McGown, A. J.; Kerber, W. D.; Fujii, H.; Goldberg, D. P. *J. Am. Chem. Soc.* **2009**, *131*, 8040–8048. (o) Company, A.; Feng, Y.; Guell, M.; Ribas, X.; Luis, J. M.; Que, L., Jr.; Costas, M. *Chem.—Eur. J.* **2009**, *15*, 3359–3362. (p) Franke, A.; Wolak, M.; van Eldik, R. *Chem.—Eur. J.* **2009**, *15*, 10182–10198. (q) Hessenauer-Ilcheva, N.; Franke, A.; Wolak, M.; Higuchi, T.; van Eldik, R. *Chem.—Eur. J.* **2009**, *15*, 12447–12459.

(18) (a) Gross, Z.; Nimri, S. *Inorg. Chem.* **1994**, *33*, 1731–1732. (b) Czarnecki, K.; Nimri, S.; Gross, Z.; Proniewicz, L. M.; Kincaid, J. R. *J. Am. Chem. Soc.* **1996**, *118*, 2929–2935. (c) Gross, Z. *J. Biol. Inorg. Chem.* **1996**, *1*, 368–371. (d) Gross, Z.; Nimri, S.; Barzilay, C. M.; Simkhovich, L. *J. Biol. Inorg. Chem.* **1997**, *2*, 492–506.

(19) (a) Nam, W.; Lim, M. H.; Oh, S.-Y.; Lee, J. H.; Lee, H. J.; Woo, S. K.; Kim, C.; Shin, W. *Angew. Chem., Int. Ed.* **2000**, *39*, 3646–3649. (b) Sastri, C. V.; Park, M. J.; Ohta, T.; Jackson, T. A.; Stubna, A.; Seo, M. S.; Lee, J.; Kim, J.; Kitagawa, T.; Münck, E.; Que, L., Jr.; Nam, W. *J. Am. Chem. Soc.* **2005**, *127*, 12494–12495. (c) Sastri, C. V.; Lee, J.; Oh, K.; Lee, Y. J.; Lee, J.; Jackson, T. A.; Ray, K.; Hirao, H.; Shin, W.; Halfen, J. A.; Kim, J.; Que, L., Jr.; Shaik, S.; Nam, W. *Proc. Natl. Acad. Sci. U.S.A.* **2007**, *104*, 19181–19186. (d) Kang, Y.; Chen, H.; Jeong, Y. J.; Lai, W.; Bae, E. H.; Shaik, S.; Nam, W. *Chem.—Eur. J.* **2009**, *15*, 10039–10046.

(20) (a) Mayer, J. M. *Acc. Chem. Res.* **1998**, *31*, 441–450. (b) Mayer, J. M. *Annu. Rev. Phys. Chem.* **2004**, *55*, 363–390. (c) Mader, E. A.; Manner, V. W.; Markle, T. F.; Wu, A.; Franz, J. A.; Mayer, J. M. *J. Am. Chem. Soc.* **2009**, *131*, 4335–4345.

(21) (a) Kaizer, J.; Klinker, E. J.; Oh, N. Y.; Rohde, J.-U.; Song, W. J.; Stubna, A.; Kim, J.; Münck, E.; Nam, W.; Que, L., Jr. *J. Am. Chem. Soc.* **2004**, *126*, 472–473. (b) Yoon, J.; Wilson, S. A.; Jang, Y. K.; Seo, M. S.; Nehru, K.; Hedman, B.; Hodgson, K. O.; Bill, E.; Solomon, E. I.; Nam, W. *Angew. Chem., Int. Ed.* **2009**, *48*, 1257–1260. (c) Lansky, D. E.; Goldberg, D. P. *Inorg. Chem.* **2006**, *45*, 5119–5125. (d) Bell, S. R.; Groves, J. T. *J. Am. Chem. Soc.* **2009**, *131*, 9640–9641.

(22) *Jaguar 7.6*; Schrödinger, LLC.: New York, NY, 2007.

(23) Frisch, M. J.; et al. *Gaussian 03*, revision C.02; Gaussian, Inc.: Wallingford, CT, 2004.

(24) (a) Becke, A. D. *J. Chem. Phys.* **1993**, *98*, 5648–5652. (b) Lee, C.; Yang, W.; Parr, R. G. *Phys. Rev. B* **1988**, *37*, 785–789.

(25) (a) Kumar, D.; de Visser, S. P.; Shaik, S. *Chem.—Eur. J.* **2005**, *11*, 2825–2835. (b) de Visser, S. P.; Oh, K.; Han, A.-R.; Nam, W. *Inorg. Chem.* **2007**, *46*, 4632–4641.

(26) Shaik, S.; Kumar, D.; de Visser, S. P. *J. Am. Chem. Soc.* **2008**, *130*, 10128–10140.

(27) Olsen, L.; Rydberg, P.; Rod, T. H.; Ryde, U. *J. Med. Chem.* **2006**, *49*, 6489–6499.

(28) (a) Kumar, D.; de Visser, S. P.; Shaik, S. *J. Am. Chem. Soc.* **2003**, *125*, 13024–13025. (b) Kumar, D.; de Visser, S. P.; Sharma, P. K.; Cohen, S.; Shaik, S. *J. Am. Chem. Soc.* **2004**, *126*, 1907–1920. (c) de Visser, S. P. *Chem.—Eur. J.* **2006**, *12*, 8168–8177.

(29) Porro, C. S.; Kumar, D.; de Visser, S. P. *Phys. Chem. Chem. Phys.* **2009**, *11*, 10219–10226.

(30) (a) de Visser, S. P. *Chem.—Eur. J.* **2008**, *14*, 4533–4541. (b) de Visser, S. P. *Coord. Chem. Rev.* **2009**, *253*, 754–768.

(31) (a) de Visser, S. P.; Tahsini, L.; Nam, W. *Chem.—Eur. J.* **2009**, *15*, 5577–5587. (b) Kumar, D.; Tahsini, L.; de Visser, S. P.; Kang, H. Y.; Kim, S. J.; Nam, W. *J. Phys. Chem. A* **2009**, *113*, 11713–11722.

(32) (a) Hay, P. J.; Wadt, W. R. *J. Chem. Phys.* **1985**, *82*, 270–283. (b) Hehre, W. J.; Ditchfield, R.; Pople, J. A. *J. Chem. Phys.* **1972**, *56*, 2257–2261.

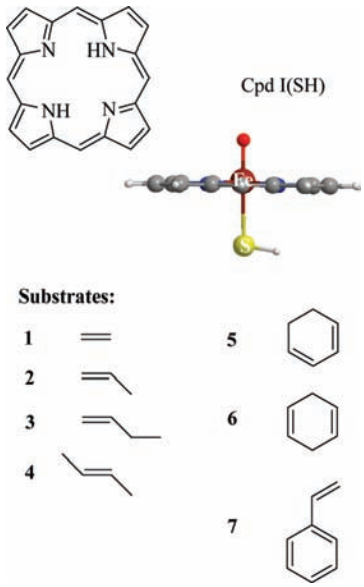

Figure 2. Model oxidant [Cpd I(SH)] and epoxidation substrates studied in this work.

set on iron (including Effective Core Potential) and 6-311+G* on the remaining atoms, basis set B2. Energies reported in this work were obtained with basis set B2 and corrected with zero-point energies from basis set B1 unless otherwise noted. To test whether the basis set affects the optimized geometries and/or energies, we reoptimized the 1-butene epoxidation mechanism by ^{4,2}Cpd I(SH) using basis set B2 followed by an analytical frequency calculation at this level. These studies gave only minor geometric and energetic differences from those done with the smaller basis set; hence basis set B1 was used for geometry optimizations and frequencies for the remaining work, while single-point calculations were done with basis set B2.

The effect of the environment was investigated by single-point calculations in *Jaguar* at UB3LYP/B2 with the self-consistent reaction field model using a dielectric constant of $\varepsilon = 5.7$ and a probe radius of 2.72 Å. These studies did not affect the trends presented in this work (Supporting Information Figure S7); therefore, we will focus in the main text on the gas-phase results only.

Cpd I of P450 was abbreviated as iron-protoporphyrin IX with a distal oxo group and axial thiolate ligand, designated Cpd I(SH);[33] see Figure 2. In this work we studied the substrate epoxidation by a model of Cpd I of P450 using a range of typical substrates. Furthermore, a comparison is made with other heme and nonheme iron(IV)-oxo oxidants. To distinguish the different iron(IV)-oxo oxidants, we will give the axial ligand of the oxidant in parentheses of Cpd I; i.e. Cpd I(SH) is designated as the iron(IV)-oxo porphyrin cation radical species of a P450 model described by a thiolate axial ligand. Cpd I(SH) appears in almost degenerate doublet and quartet spin states; therefore, all calculations were done for both spin state surfaces. We studied substrate epoxidation by Cpd I(SH) with seven olefins: ethene (**1**), propene (**2**), 1-butene (**3**), *trans*-2-butene (**4**), 1,3-cyclohexadiene (**5**), 1,4-cyclohexadiene (**6**), and styrene (**7**). Although ethene epoxidation by Cpd I(SH) was studied before,[34] we redid these calculations using the methods described above. Data for propene and styrene epoxidation by Cpd I(SH) were taken from the literature.[25a,35]

Ionization energies of substrates (IE_{Sub}) represent adiabatic ionization energies and were calculated with the same procedures mentioned above, namely geometry optimizations using basis set B1, while energies are taken from single-point calculations with basis set B2 corrected for ZPE with basis set B1. These calculated values reproduce experimentally determined IE values excellently; see Supporting Information.[36]

Reorganization energies (RE) were calculated as before from the difference in energy of the substrate in the transition state geometry and its fully relaxed structure.[26] The bond dissociation energy of the O−H bond in the iron(IV)-hydroxo complex with ligand L (BDE_{OH}) was calculated from eq 2 using fully optimized geometries at the B3LYP/B1 level of theory and energies from B3LYP/B2//B3LYP/B1 including ZPE at basis set B1.

$$\text{Cpd I(L)} + \text{H}^{\bullet} \rightarrow \text{Fe}^{\text{IV}}\text{OH(L)} + \text{BDE}_{\text{OH}} \qquad (2)$$

In addition, we also tested trends of epoxidation reactions with varying oxidants but with the same substrate (propene), namely Cpd I(SH), Cpd I(OH), Cpd I(Cl), Cpd I(ImP), Cpd I(C*c*P), Cpd I(TauD), and Fe^{IV}═O(TMCS)$^+$; see Figure 3. The first four of these oxidants are iron(IV)-oxo porphyrin cation radical models with the axial ligand of these systems written in parentheses. Cpd I(C*c*P) and Cpd I(TauD) represent enzyme active site models of the iron(IV)-oxo species of the enzymes cytochrome *c* peroxidase (C*c*P) and taurine/α-ketoglutarate dioxygenase (TauD). Data for propene epoxidation by Cpd I(Cl), Cpd I(ImP), Cpd I(TauD), and Fe^{IV}═O(TMCS)$^+$ were taken from the literature.[37] Cpd I(ImP) is an iron(IV)-oxo porphyrin cation radical oxidant with an imidazole ligand whereby the atom bound to the metal is replaced by phosphorus, whereas Fe^{IV}═O(TMCS)$^+$ represents a nonheme iron(IV)-oxo complex with TMCS = 1-mercaptoethyl-4,8,11-trimethyl-1,4,8,11-tetraaza cyclotetradecane as a pentadentate ligand.

To find out whether a thiolate axial ligand correctly mimics the cysteinate ligand in P450 enzymes, we ran an extra set of calculations where we calculated the BDE_{OH} value for three different models, namely using SH^-, SCH_3^-, and a large model containing a peptide chain of cysteinate connected to two glycine amino acids, $CysGlyGly^-$. In the latter structure the hydrogen bonding interactions of amide protons to the sulfur atom of cysteinate [NH---S interactions] in the enzyme are included that determine the electron-donating ability of the axial ligand. BDE_{OH} values of 88.9, 87.4, and 88.95 kcal mol^{-1} were obtained for Cpd I(SH), Cpd I(SCH_3), and Cpd I(CysGlyGly), respectively. Therefore, thiolate is a faithful mimic of the active species of P450 enzymes. Further calculations on the relative BDE_{OH} values of Cpd I(OH) and Cpd I(OCH_3) predicted values of 97.4 versus 99.5 kcal mol^{-1}, respectively, which implies that these two axial ligand systems will show similar reactivity patterns with the substrates discussed in this work.

Results and Discussion

Substrate Epoxidation by Cpd I(SH). The active species of P450 enzymes is elusive but is expected to resemble that of chloroperoxidase enzymes, which is well characterized spec-

(33) de Visser, S. P.; Shaik, S.; Sharma, P. K.; Kumar, D.; Thiel, W. *J. Am. Chem. Soc.* **2003**, *125*, 15779–15788.
(34) de Visser, S. P.; Ogliaro, F.; Harris, N.; Shaik, S. *J. Am. Chem. Soc.* **2001**, *123*, 3037–3047.
(35) (a) de Visser, S. P.; Ogliaro, F.; Sharma, P. K.; Shaik, S. *Angew. Chem., Int. Ed.* **2002**, *41*, 1947–1951. (b) de Visser, S. P.; Ogliaro, F.; Sharma, P. K.; Shaik, S. *J. Am. Chem. Soc.* **2002**, *124*, 11809–11826.
(36) (a) Lias, S. G. Ionization energy evaluation. In *NIST Chemistry Webbook, NIST Standard Reference Database Number 69*; Linstrom, P. J., Mallard, W. G., Eds.; National Institute of Standards and Technology: Gaithersburg, MD. 20899 (http://webbook.nist.gov, 2009). (b) Kimura, K.; Katsumata, S.; Achiba, Y.; Yamazaki, T.; Iwata, S. *Handbook of HeI photoelectron spectra of fundamental organic molecules: ionization energies, ab initio assignments, and valence electronic structure for 200 molecules*; Japan Scientific Society Press: Tokyo, 1981.
(37) (a) de Visser, S. P. *J. Biol. Inorg. Chem.* **2006**, *11*, 168–178. (b) de Visser, S. P. *J. Am. Chem. Soc.* **2006**, *128*, 9813–9824. (c) de Visser, S. P. *J. Am. Chem. Soc.* **2006**, *128*, 15809–15818. (d) de Visser, S. P. *J. Phys. Chem. B* **2007**, *111*, 12299–12302. (e) de Visser, S. P. *Angew. Chem., Int. Ed.* **2006**, *45*, 1790–1793.

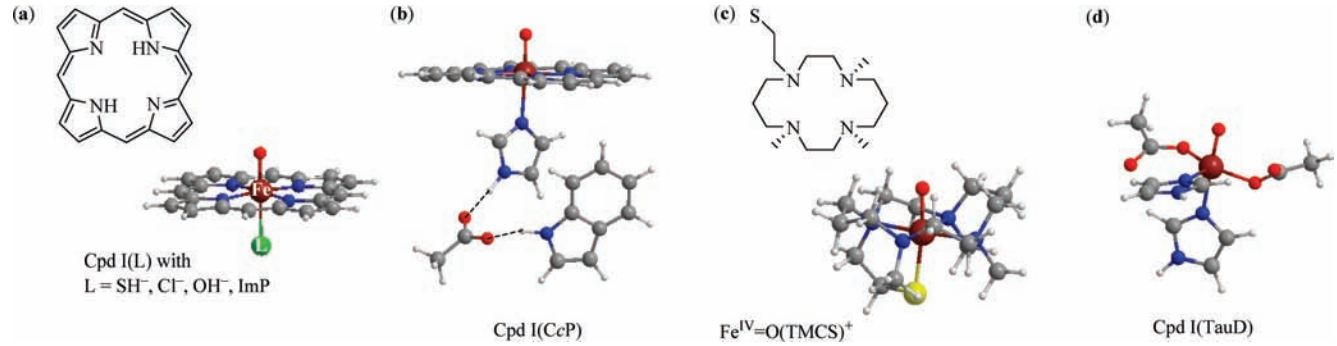

Figure 3. Iron(IV)-oxo oxidants studied in the reaction with propene.

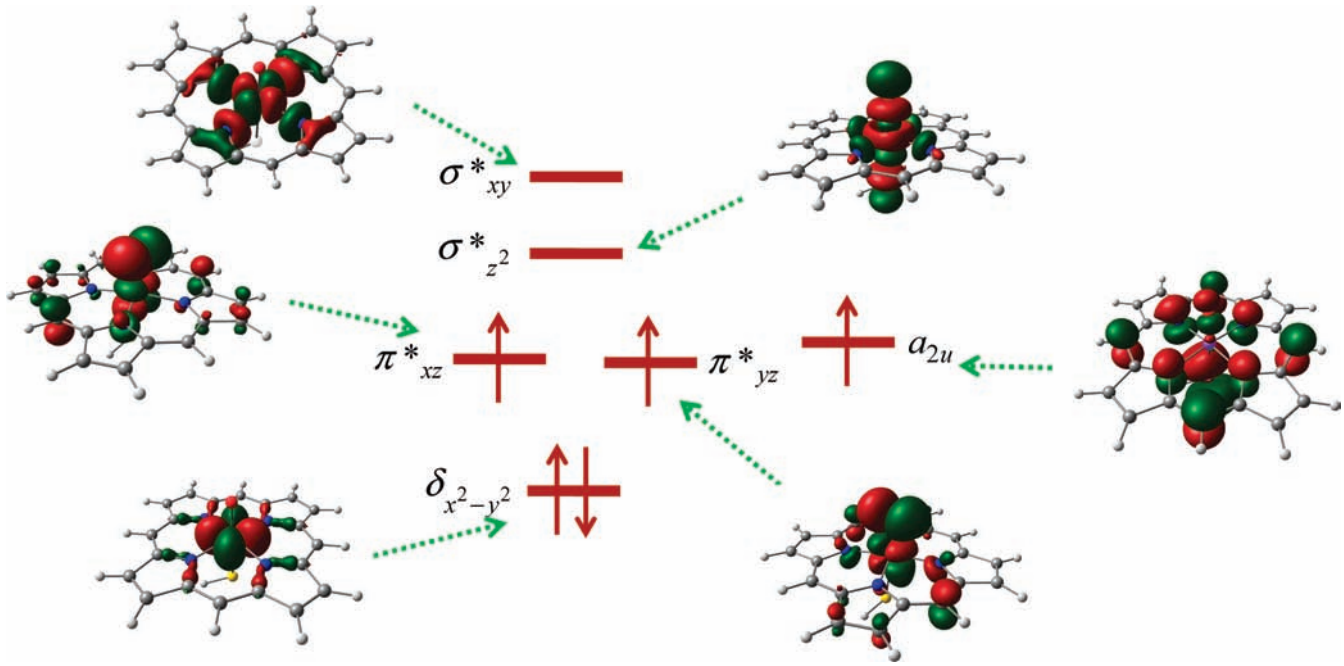

Figure 4. High-lying occupied and low-lying virtual orbitals of Cpd I(SH).

troscopically and computationally.[38] Substrate epoxidation by Cpd I of P450 takes place via two-state-reactivity patterns on competing doublet and quartet spin state surfaces[39] with electronic configuration $\delta_{x^2-y^2}{}^2\ \pi^*_{xz}{}^1\ \pi^*_{yz}{}^1\ a_{2u}{}^1$ as shown in Figure 4. These orbitals are dominated by the 3*d* metal contributions, whereby the lowest one of those is the nonbonding $\delta_{x^2-y^2}$ orbital in the plane of the heme that is doubly occupied in all structures discussed in this work. Higher in energy and singly occupied is a pair of orthogonal π^*_{xz} and π^*_{yz} orbitals for the antibonding combination of a 3*d* orbital on iron with a 2*p* orbital on the oxo group. The lowest two virtual orbitals with metal contributions are the σ^*_{xy} orbital for the antibonding interactions of the metal with the porphyrin nitrogen atoms and the $\sigma^*_{z^2}$ orbital for the antibonding interactions with the axial and distal ligands. Also singly occupied is a porphyrin based orbital that in D_{4h} symmetry has the label a_{2u}. Since the interaction between the two π^* orbitals and the a_{2u} orbital is small, the doublet and quartet spin states are close in energy and lead to reactivity patterns on the two spin state surfaces with different reaction barriers.[39]

The other oxidants given in Figure 3 have similar sets of valence orbitals, and all heme oxidants, apart from Cpd I(C*c*P), have the same orbital occupation. Cpd I(C*c*P) has a singly occupied π-orbital on the axial Trp residue rather than a porphyrin radical. The nonheme iron(IV)-oxo oxidants, Fe^{IV}═O(TMCS)$^+$ and Cpd I(TauD), were calculated in the quintet spin state with $\delta_{x^2-y^2}{}^1\ \pi^*_{xz}{}^1\ \pi^*_{yz}{}^1\ \sigma^*_{xy}{}^1$ occupation.

A typical example of a reaction profile of substrate epoxidation by Cpd I(SH) is given in Figure 5 for the epoxidation of 1-butene (**3**) by Cpd I(SH); all other epoxidation reactions studied in this work gave similar reaction profiles; see Supporting Information. The reaction starts from ^{4,2}Cpd I(SH), whereby both states are within 0.1 kcal mol^{-1}. The initial and rate-determining step in the reaction mechanism is C−O bond formation to give a radical intermediate (**I**) via a transition state $\mathbf{TS}_E$. A subsequent ring-closure barrier ($\mathbf{TS}_{rc}$) separates the intermediate complexes from products (**P**). Generally, the ring-

(38) (a) Rutter, R.; Hager, L. P.; Dhonau, H.; Hendrich, M.; Valentine, M.; Debrunner, P. *Biochemistry* **1984**, *23*, 6809–6816. (b) Palcic, M. M.; Rutter, R.; Araiso, T.; Hager, L. P.; Dunford, H. B. *Biochem. Biophys. Res. Commun.* **1980**, *94*, 1123–1127. (c) Egawa, T.; Proshlyakov, D. A.; Miki, H.; Makino, R.; Ogura, T.; Kitagawa, T.; Ishimura, Y. *J. Biol. Inorg. Chem.* **2001**, *6*, 46–54. (d) Hosten, C. M.; Sullivan, A. M.; Palaniappan, V.; Fitzgerald, M. M.; Terner, J. *J. Biol. Chem.* **1994**, *269*, 13966–13978. (e) Kim, S. H.; Perera, R.; Hager, L. P.; Dawson, J. H.; Hoffman, B. M. *J. Am. Chem. Soc.* **2006**, *128*, 5598–5599. (f) Stone, K. L.; Behan, R. K.; Green, M. T. *Proc. Natl. Acad. Sci. U.S.A.* **2006**, *103*, 12307–12310.
(39) Shaik, S.; de Visser, S. P.; Ogliaro, F.; Schwarz, H.; Schröder, D. *Curr. Opin. Chem. Biol.* **2002**, *6*, 556–567.

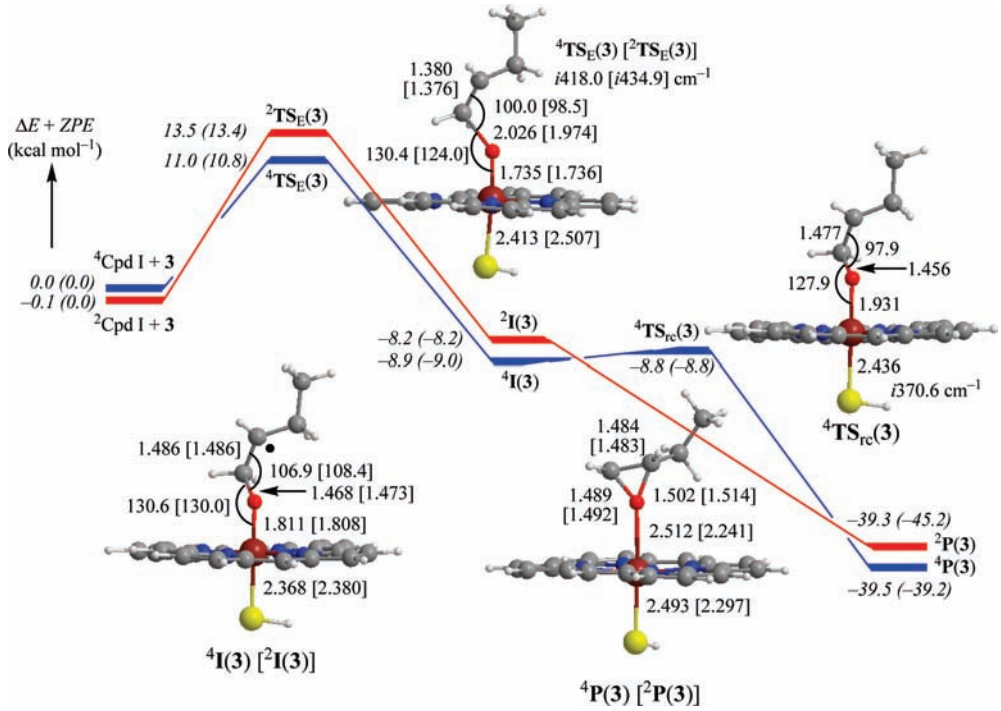

Figure 5. Reaction profile of 1-butene (**3**) epoxidation by ^{4,2}Cpd I(SH) with energies in kcal mol^{-1}. Also shown are optimized geometries of the critical points along the reaction mechanism obtained at UB3LYP/B1 with distances in angstroms, angles in degrees, and the value of the imaginary frequency in the transition state in wave numbers. Energies reported outside parentheses are obtained with basis set B2 on UB3LYP/B1 optimized geometries and contain ZPE corrections with basis set B1. Inside parentheses are reported energies (including ZPE) calculated at UB3LYP/B2 after a UB3LYP/B2 geometry optimization and frequency.

Table 1. Relative Energies of Critical Points along the Mechanism of Epoxidation of Substrates by Cpd I(SH) and Calculated Values of the Reorganization Energy (RE) and Ionization Energy (IE) of the Substrates[a]

	Substrate	^{4}TS$_E$	^{4}I	^{2}TS$_E$	^{2}I	RE$_{HS}$	IE$_{Sub}$
1	ethene	14.13	−5.95	14.29	−5.52	2.80	238.9
2	propene	13.13	−6.48	12.60	−6.27	2.93	219.7
3	1-butene	11.06	−8.86	13.52	−8.21	1.29	214.8
4	*trans*-2-butene	10.85	−6.80	10.03	*b*	2.96	203.7
5	1,3-cyclohexadiene	7.90	−19.29	9.42	*b*	2.91	181.4
6	1,4-cyclohexadiene	11.94	−3.96	13.12	*b*	5.15	194.5
7	styrene	8.95	−15.13	9.53	−14.70	3.25	187.7

[a] All energies are in kcal mol^{-1}, relative to isolated reactants and obtained with basis set B2 including ZPE with basis set B1. [b] No low-spin intermediate found; instead the reaction gives products directly.

closure barrier is small or negligible on the low-spin surface and somewhat higher on the high-spin surface.[34] This mechanism shows similarities to aliphatic hydroxylation mechanisms discussed before that gave a stepwise mechanism with an initial and rate-determining hydrogen abstraction step.[8] Similar to the epoxidation mechanism, in aliphatic hydroxylation reactions the rebound step is either negligible or barrierless on the low-spin surface, whereas it proceeds with a significantly higher barrier on the high-spin surface.[40] To ascertain that the optimized geometries and relative energies are not influenced by the choice of the basis set in the calculations, we repeated the geometry optimizations for the complete reaction mechanism shown in Figure 5 using the UB3LYP/B2 method followed by an analytical frequency at this level. As follows, the energies of the various steps in the reaction mechanism are generally within 0.2 kcal mol^{-1} of those obtained at UB3LYP/B2//UB3LYP/B1 with ZPE included from the UB3LYP/B1 results. Moreover, the optimized geometries are very similar to those found with the smaller basis set generally with deviations well below 0.010 Å for distances and less than 1° for angles and dihedrals (Supporting Information). It appears, therefore, that relative energies obtained from geometry and frequency calculations at UB3LYP/B1 are reliable and single-point energy calculations at the UB3LYP/B2 level of theory give sufficiently accurate results. Accordingly, we have used the latter method for the remaining calculations described in this work.

Table 1 summarizes the relative energies of ^{4,2}**TS**$_E$ and ^{4,2}**I** for all substrate epoxidation reactions calculated with Cpd I(SH), while optimized geometries of ^{4,2}**TS**$_E$ are shown in Figure 6. The lowest epoxidation barriers are obtained with 1,3-cyclohexadiene and styrene, while the highest barriers are found for ethene (**1**). The values of ^{4,2}**TS**$_E$(**1**) are in good agreement with those reported in the literature[34] although calculated with slightly different methods. In three cases we were unable to locate a radical intermediate in the low-spin state (^{2}**I**), namely using *trans*-2-butene, 1,3-cyclohexadiene, and 1,4-cyclohexadiene as substrates, where the geometry optimization fell to the product complexes instead. In all other cases an optimized geometry

(40) (a) Shaik, S.; Cohen, S.; de Visser, S. P.; Sharma, P. K.; Kumar, D.; Kozuch, S.; Ogliaro, F.; Danovich, D. *Eur. J. Inorg. Chem.* **2004**, 207–226. (b) Siegbahn, P. E. M.; Borowski, T. *Acc. Chem. Res.* **2006**, *39*, 729–738.

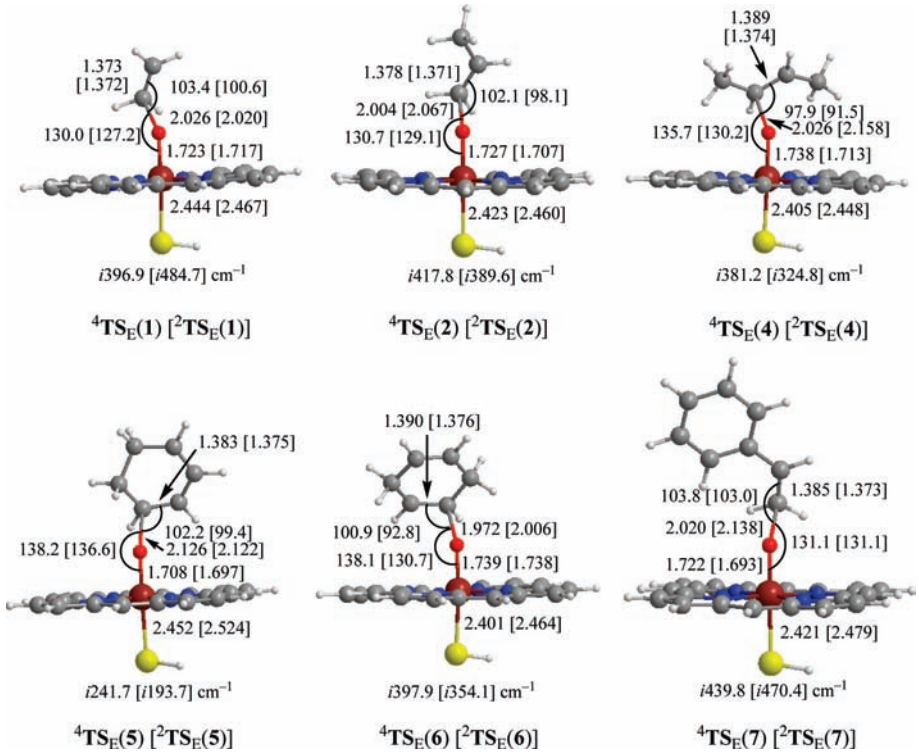

Figure 6. Optimized transition state geometries, ^{4,2}**TS**$_E$, as obtained with *Jaguar* with B3LYP for substrates: ethene (**1**), propene (**2**), *trans*-2-butene (**4**), 1,3-cyclohexadiene (**5**), 1,4-cyclohexadiene (**6**), and styrene (**7**). Bond lengths are in angstroms, angles in degrees, and the imaginary frequency in the transition state in wave numbers. Structures for 1-butene are displayed in Figure 5 above.

for a doublet spin intermediate was found, but these structures are short-lived with negligible ring-closure barriers leading to products. Therefore, the low-spin mechanism can be regarded as concerted via ^{2}**TS**$_E$, although this is not a symmetric transition state since it contains significant radical character and unequal C−O distances.

Generally the quartet and doublet spin transition state structures are close in energy, typically within 2 kcal mol^{-1}, which is not surprising since the same electron transfer processes take place, whereby an electron is transferred from the substrate into the a_{2u} orbital to give a radical intermediate with the metal in oxidation state Fe(IV) and a closed shell porphyrin macrocycle. Earlier epoxidation studies showed that in the gas phase the barriers leading to intermediates with an iron(III) coupled to a porphyrin cation radical are higher in energy.[35] Optimized geometries of epoxidation barriers in Figure 6 show typical features observed before. In most cases the transition state is early with relatively long C−O distances of ∼2 Å and short C−C bonds of 1.37−1.39 Å. Attempts to correlate the geometric features of the transition states with barrier height gave no clear relationships (see Supporting Information Figures S1−S6).

In principle, the highest occupied molecular orbital of an olefin is typically a π-orbital along a double bond; hence ionizing an electron from this bond should correspond to the strength of this double bond. To test whether the barrier heights of substrate epoxidation by Cpd I(SH) are connected to the ionization potential of the substrate, we calculated epoxidation mechanisms and substrate ionization potentials. In Figure 7, we display the correlation between epoxidation barrier height in the quartet spin state with substrate ionization energy (IE) for the reactions with Cpd I(SH) as an oxidant. The correlation between barrier height and substrate IE is fair with a correlation coefficient $R^2 = 0.80$. In previous studies we showed that a

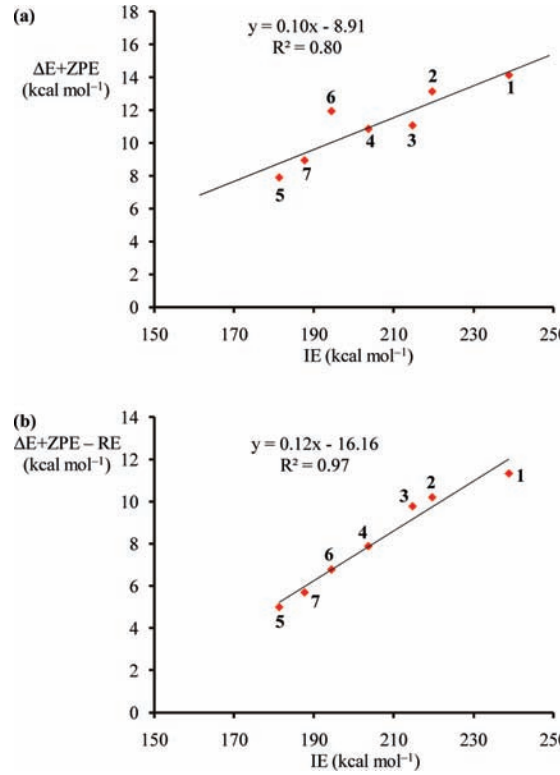

Figure 7. Correlation of epoxidation barrier height with the IE of the substrate without inclusion of the reorganization energy (a) or with inclusion of the RE (b). Substrates studied are: ethene (**1**), propene (**2**), 1-butene (**3**), *trans*-2-butene (**4**), 1.3-cyclohexadiene (**5**), 1,4-cyclohexadiene (**6**), and styrene (**7**).

better correlation can be achieved through inclusion of an RE contribution.[26] Indeed, a significant improvement is found

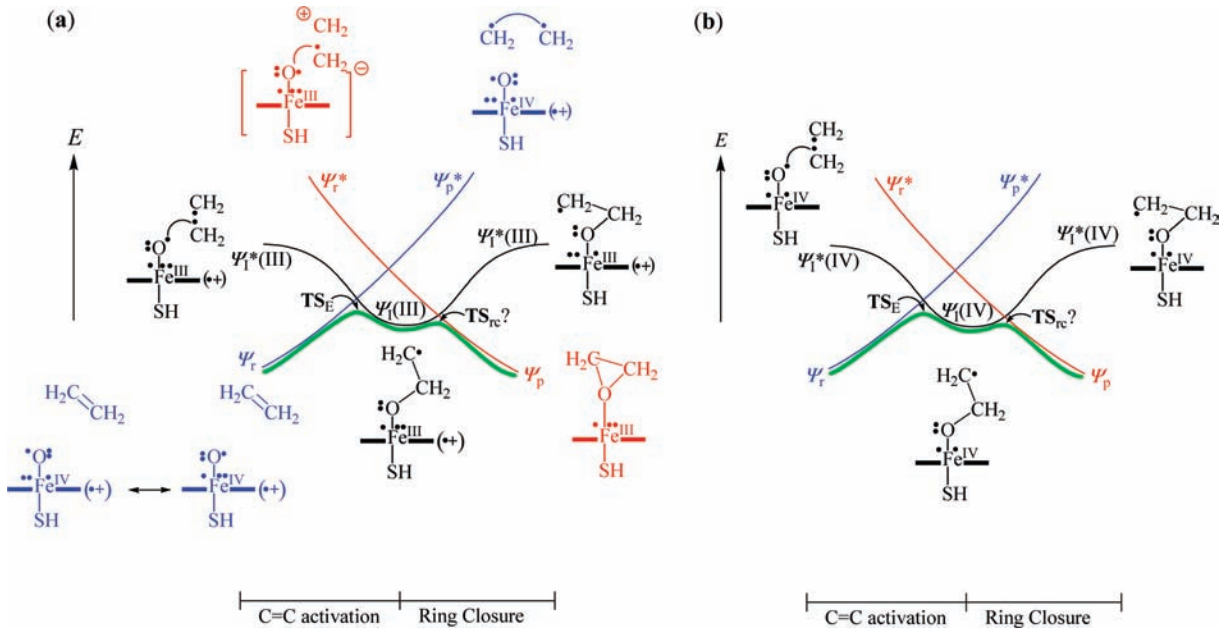

Figure 8. Valence bond curve crossing diagram of ethene epoxidation by Cpd I of P450 via **I**(Fe^{III}) (a) or **I**(Fe^{IV}) (b).

(Figure 7b) and the correlation coefficient rises to $R^2 = 0.97$, which proves that substrate epoxidation reactions are connected to the ionization potential of the substrates and that IE is a good representation of the π-bond strength of the olefin. To test the effect of a local environment on the barrier heights we recalculated the energies in a dielectric constant of $\epsilon = 5.7$ (Figure S7); however, the displayed trend only shows minor differences with the one reported in Figure 7a.

Origin of Correlation between Epoxidation Barrier and Ionization Energy (IE). The trends displayed in Figure 7 show that the barrier of olefin epoxidation by Cpd I(SH) correlates with the ionization energy of the substrate. Since, the highest occupied molecular orbital (HOMO) in all substrates is a π-orbital representing the double bond of the olefin, this implies that the energy of converting the double bond of the olefin into a single bond determines the barrier height of epoxidation. Recently, we explained substrate hydroxylation by heme and nonheme iron(IV)-oxo oxidants with a valence bond (VB) curve crossing diagram and thermodynamic cycles, and here we will follow an analogous approach to describe substrate epoxidation.[26,41]

Figure 8 displays the VB curve crossing diagram for substrate epoxidation by Cpd I(SH), where we use ethene as the olefin, but for other substrates analogous diagrams can be drawn. The relevant valence π-electrons in Figure 8 are displayed with a dot. The VB curve crossing diagram starts bottom left (in blue) with the reactants that appear in a reactant wave function Ψ_r. Thus, Cpd I(SH) has orbital occupation $\delta_{x^2-y^2}^2\ \pi_{xz}^2\ \pi_{yz}^2\ \pi^*_{xz}{}^1\ \pi^*_{yz}{}^1\ a_{2u}{}^1$, which gives rise to a spin density of approximately one on the iron, one on the oxygen atom, and one spread out over the porphyrin and axial ligands; hence we depict one unpaired electron next to the iron, one next to the oxo group, and one on the porphyrin macrocycle. In addition there are two electrons in the π-bond of the double bond of the substrate. This wave function connects to an excited state in the product geometry (Ψ_p*). In a similar way, the product wave function is represented by Ψ_p and has orbital occupation $\delta_{x^2-y^2}^2\ \pi^*_{xz}{}^2\ \pi^*_{yz}{}^1\ a_{2u}{}^2$ for $^2\mathbf{P}_E$ or $\delta_{x^2-y^2}^2\ \pi^*_{xz}{}^1\ \pi^*_{yz}{}^1\ \sigma^*_{z^2}{}^1\ a_{2u}{}^2$ for $^4\mathbf{P}_E$. The product wave function connects to an excited state wave function Ψ_r* in the geometry of the reactants. Thus, the point where the Ψ_r and Ψ_p wave functions cross leads to an avoided crossing and a transition state for the reaction. However, the reactant and product wave function are crossed by a third wave function curve that represents the intermediate complexes. In principle, there are two possibilities of an intermediate complex, namely one with the $Fe^{III}(Por^{+\bullet})(SH)OCH_2CH_2^{\bullet}$ configuration, designated **I**(Fe^{III}), and the other with the $Fe^{IV}(Por)(SH)OCH_2CH_2^{\bullet}$ configuration or **I**(Fe^{IV}). Gas-phase DFT calculations usually predict the Fe^{IV} complexes to be the lowest in energy,[34,35] but in enzymatic models often the Fe^{III} complexes are lowest lying.[42] Nevertheless, we show both VB diagrams in Figure 8, and the calculated trends on the Fe^{III} and Fe^{IV} surfaces should be similar. The crossing of the intermediate wave function, that is Ψ_I(III) or Ψ_I(IV), with the reactant wave function gives rise to a C−O bond formation barrier ($\mathbf{TS}_E$), while its crossing with the product wave function leads to the ring-closure transition state ($\mathbf{TS}_{rc}$). Thus, these VB curve crossing diagrams shown in Figure 8 explain why the reactions are stepwise via a radical intermediate. This quantitative model supports the reaction mechanisms calculated for the structures shown in Table 1 and the landscape depicted in Figure 5.

In VB theory the height of the avoided crossing can be determined from the excitation energy values in the reactant geometry;[43] see Figure 9. Thus, the crossing of reactant and intermediate wave functions Ψ_r and Ψ_I leads to an avoided crossing and a transition state for C−O bond formation in the epoxidation reaction. The curve crossing takes place at ΔE_c above the energy of the reactants, but the barrier height $\mathbf{TS}_E$ is a factor B below this crossing point at an energy $\Delta E^{\ddagger}$. This factor B represents the resonance energy of the molecule in the

(41) (a) Latifi, R.; Bagherzadeh, M.; de Visser, S. P. *Chem.—Eur. J.* **2009**, *15*, 6651–6662. (b) de Visser, S. P. *J. Am. Chem. Soc.* **2010**, *132*, 1087–1097.

(42) Schöneboom, J. C.; Cohen, S.; Lin, H.; Shaik, S.; Thiel, W. *J. Am. Chem. Soc.* **2004**, *126*, 4017–4034.

(43) (a) Shaik, S. S. *J. Am. Chem. Soc.* **1981**, *103*, 3692–3701. (b) Shaik, S.; Shurki, A. *Angew. Chem., Int. Ed.* **1999**, *38*, 586–625.

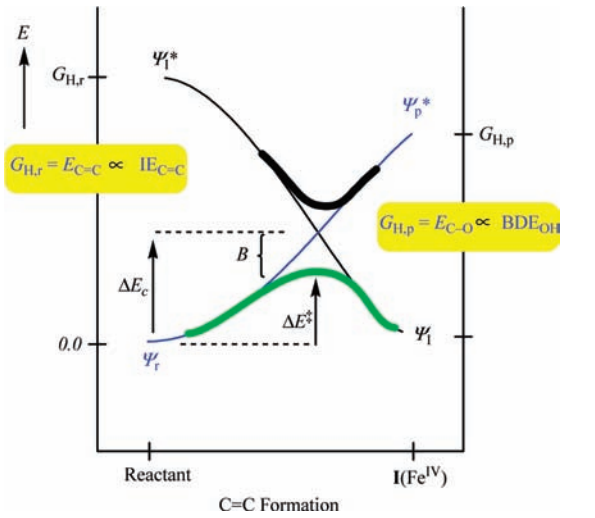

Figure 9. VB curve crossing diagram for the C−O bond formation step in the epoxidation reaction.

Table 2. DFT and VB Calculated Epoxidation Barrier Heights[a]

substrate	^{4}**TS**$_E$	RE$_{HS}$	$\Delta E_{DFT}^{\ddagger}$ [b]	$\Delta E_{VB}^{\ddagger}$
ethene	14.13	2.80	11.33	9.10
propene	13.13	2.93	10.21	9.07
1-butene	11.06	1.29	9.78	8.62
trans-2-butene	10.85	2.96	7.89	8.55
1,3-cyclohexadiene	7.90	2.91	5.00	5.50
1,4-cyclohexadiene	11.94	5.15	6.78	8.87
styrene	8.95	3.25	5.70	6.34

[a] All values in kcal mol^{-1}. [b] $\Delta E_{DFT}^{\ddagger} = \Delta E + ZPE(^4\mathbf{TS}_E) - RE_{HS}$.

transition state. The promotion gap (G_H) or excitation energy from the reactant wave function to the intermediate wave function in the reactants geometry is proportional to a fraction f of the curve crossing point via $\Delta E_c = f G_H$ to give

$$\Delta E^{\ddagger} = fG_H - B \qquad (3)$$

As follows from Figures 8 and 9, the promotion gap G_H is proportional to the energy to break the π-bond of the olefin. Since the IE of the olefins studied here is correlated with the expulsion of an electron from the double bond, this implies that the barrier height $\mathbf{TS}_E$ should correlate with IE as well, as indeed shown above in Figure 7. Therefore, the VB curve crossing diagram explains the correlation of barrier height with IE. This makes substrate epoxidation fundamentally different from aliphatic hydroxylation, where the VB curve crossing diagram connected the barrier with the strength of the C−H bond of the substrate.

To test whether the VB method described in Figure 9 can predict epoxidation barrier heights from empirical data, we used eq 3 above together with estimated values for G_H and B. The promotion gap was estimated as twice the first excitation energy of the substrate, which corresponds to a $\pi-\pi^*$ excitation in the double bond, i.e. is proportional to the dissociation energy of the double bond, $D_{C=C}$. Excitation energies were calculated using time-dependent DFT on the optimized reactant geometries using basis set B2. The resonance energy (B) was taken as half the energy of the C=C bond energy. Together with the RE corrected barrier heights, f was calculated using the values for G_H and B. The average value of f ($f_{AV} = 0.299 \pm 0.008$) together with G_H and B gave the VB calculated barrier heights ($\Delta E_{VB}^{\ddagger}$); see Table 2. For comparison we also give the DFT calculated barrier height ($\Delta E_{DFT}^{\ddagger}$), which is the difference between $^4\mathbf{TS}_E$ and RE. In general, the agreement between $\Delta E_{DFT}^{\ddagger}$ and $\Delta E_{VB}^{\ddagger}$ is fair with a standard deviation of 1.4 kcal mol^{-1}; hence the VB estimated barriers reproduce DFT calculated barriers well and predict the correct trends.

Scheme 1. Thermodynamic Cycle for the Reaction of Cpd I(SH) with Olefin To Form a Radical Intermediate

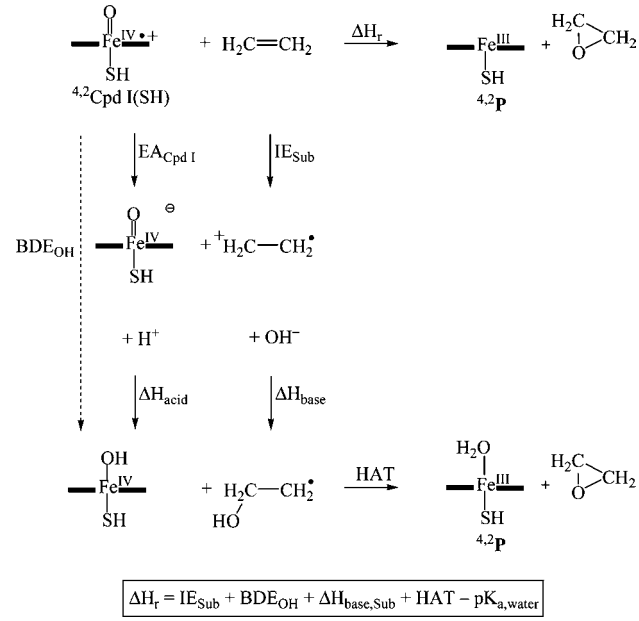

The VB diagram in Figure 9 predicts that the barrier height of substrate epoxidation is connected to the IE of the substrate through the reactant promotion gap ($G_{H,r}$), whereas the promotion gap in the radical intermediate is proportional to the energy required to form the C−O bond ($G_{H,p}$). To predict substrate epoxidation barriers, we have investigated thermodynamic cycles that ultimately correlate the C−O bond formation with barrier height. Thermodynamically, the reaction between oxidant and olefin leading to epoxide products is described in Scheme 1 and has reaction enthalpy ΔH_r. This enthalpy can be split into several components, such as the ionization energy of the substrate (IE_{Sub}) and the electron affinity of Cpd I(SH), EA_{CpdI}. As shown in eq 2, the latter is connected to the value of BDE_{OH} of Fe^{IV}(OH)(Por)(SH) via the sum of EA_{CpdI} and ΔH_{acid} (or pK_a).[44] In a similar way the OH affinity of substrate (ethene) is the sum of the IE of ethene and ΔH_{base}, Scheme 1. A final hydrogen atom transfer (HAT) between $HOCH_2CH_2^{\bullet}$ and Fe^{IV}(OH)(Por)(SH) followed by ring closure then gives an iron(III)−porphyrin complex with bound water and epoxide products. Energetically, the overall epoxidation reaction of olefins by metal-oxo complexes, therefore, is dependent on IE_{Sub}, BDE_{OH}, $\Delta H_{base}(^+CH_2-CH_2^{\bullet})$, and the HAT energy. If this thermodynamic scheme is correct, then both aliphatic hydroxylation and double bond epoxidation reactions by metal-oxo oxidants are dependent on BDE_{OH}. To test this hypothesis, we calculated a series of propene epoxidation reactions using a range of iron(IV)-oxo oxidants and compared the epoxidation barrier heights with BDE_{OH}, as described in the next section.

Propene Epoxidation by Iron(IV)-Oxo Oxidants. So far, only studies using one particular oxidant have been discussed;

(44) (a) Friedrich, L. E. *J. Org. Chem.* **1983**, *48*, 3851–3852. (b) Bordwell, F. G.; Cheng, J.-P. *J. Am. Chem. Soc.* **1991**, *113*, 1736–1743. (c) Bordwell, F. G.; Cheng, J.-P.; Ji, G.-Z.; Satish, A. V.; Zhang, X. *J. Am. Chem. Soc.* **1991**, *113*, 9790–9795.

Table 3. DFT Calculated Propene Epoxidation Barriers Using a Range of Iron(IV)-Oxo Oxidants and Calculated Values for the Electron Affinity of Cpd I($EA_{Cpd\ I}$) and BDE_{OH}

	oxidant	$^{HS}TS_E$	$EA_{Cpd\ I}$	BDE_{OH}
A	Cpd I(SH)	13.13	70.6	88.9
B	Cpd I(OH)	5.67	76.2	99.5
C	Cpd I(Cl)	12.72	79.3	87.5
D	Cpd I(ImP)	13.58	151.0	85.4
E	Cpd I(C*c*P)	15.78	147.8	83.5
F	Fe^{IV}═O(TMCS)$^+$	17.90	124.6	84.1
G	Cpd I(TauD)	4.82	53.0	95.8

[a] All data in kcal mol^{-1} obtained with basis set B2 and with ZPE included with basis set B1.

however, to generalize the trends and to prove the thermodynamic model shown in Scheme 1, we calculated a series of substrate epoxidation reactions using propene as a substrate and varying iron(IV)-oxo oxidants with heme as well as nonheme ligand systems. In principle, the VB diagram shown above predicts that the barrier height of substrate epoxidation by iron(IV)-oxo oxidants should also correlate with the energy to form the C−O bond. In principle, however, the formation of a C−O bond between a substrate and an iron(IV)-oxo complex should be proportional to the formation of an O−H bond in a reaction of an iron(IV)-oxo species with a hydrogen atom, i.e. BDE_{OH} as predicted by the thermodynamic cycle in Scheme 1. To test this hypothesis, we ran an extra set of calculations on propene epoxidation by a range of different Cpd I models, using the iron(IV)-oxo complexes shown in Figure 3 above. Propene epoxidation data for Cpd I(Cl), Cpd I(ImP), Cpd I(TauD), and Fe^{IV}═O(TMCS)$^+$ were taken from the literature.[34] Subsequently, we took the various Cpd I reactants and added a hydrogen atom to give the iron-hydroxo complexes and calculated the bond dissociation energy of the O−H bond (BDE_{OH}) for the iron-hydroxo complex using reaction 2. Calculated barrier heights, BDE_{OH}, and EA_{CpdI} data are summarized in Table 3. These oxidants have different BDE_{OH} strengths with a range spread of more than 16 kcal mol^{-1}. The lowest epoxidation barriers are obtained with Cpd I(TauD) and Cpd I(OH), which are also the oxidants with the largest BDE_{OH} values. Interestingly, no correlation between electron affinity of the oxidant (EA_{CpdI}) and barrier height is found.

Figure 10 shows propene epoxidation barriers as a function of BDE_{OH} for the seven oxidants shown in Figure 3. The correlation is reasonable and improves to $R^2 = 0.92$ when corrections for the RE are applied. Therefore, in support of the electron transfer mechanisms shown in Figure 8 and the thermodynamic cycle in Scheme 1, we have established a method to correlate the barrier height to the strength of the C−O bond formed in an epoxidation reaction through the use of BDE_{OH}. Interestingly, also aliphatic hydroxylation reactions correlate with BDE_{OH}, which means that the regioselectivity of substrate epoxidation versus hydroxylation is not determined by the oxidant but only by the electronic properties of the substrate.

The trends observed in Table 2 and Figure 10 are in excellent agreement with previous axial ligand studies of styrene epoxidation by Fe^{IV}═O(TMP$^{+\bullet}$)L, with L = F^-, $HOCH_3$, Cl^-, OAc^-, $CF_3O_2SO^-$, and ClO_4^- and with TMP = tetramesitylporphyrin.[18] Thus, calculations on Fe^{IV}═O(Por$^{+\bullet}$)L with L = F^-, Cl^-, OAc^-, and ClO_4^- give BDE_{OH} values of 93.7, 87.5, 89.5, and 83.2 kcal mol^{-1}, respectively. For the set of Fe^{IV}═O(TMP$^{+\bullet}$)L with L = F^-, Cl^-, and OAc^-, Gross and co-workers measured rate constants of styrene epoxidation of 706, 149, and 114 × 10^{-3} M^{-1} min^{-1} at −78 °C, while Fe^{IV}═O(TMP$^{+\bullet}$)ClO_4 was found to be unreactive. The trends in BDE_{OH} values are, therefore, in good agreement with the styrene epoxidation rate constants of the Gross group, where the highest rate constant was found for Fe^{IV}═O(Por$^{+\bullet}$)F and no reactivity with Fe^{IV}═O(Por$^{+\bullet}$)ClO_4. Furthermore, Fe^{IV}═O(TMP$^{+\bullet}$)Cl and Fe^{IV}═O(TMP$^{+\bullet}$)OAc have very similar BDE_{OH} values and their rate constants of styrene epoxidation are close. Consequently, experimental data support the conclusions drawn from the DFT calculations excellently.

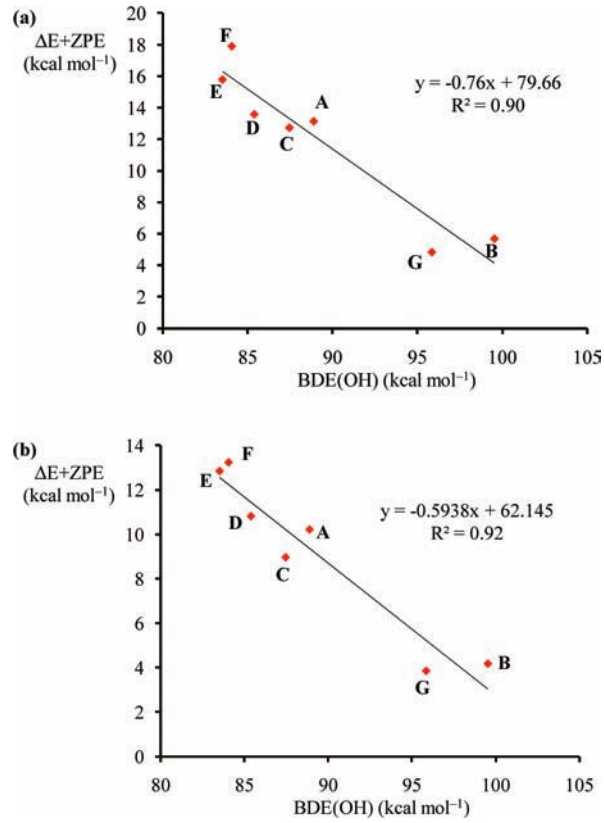

Figure 10. Correlation of propene epoxidation barrier height with BDE_{OH} of Cpd I without inclusion of the RE (a) or with inclusion of the RE (b). Oxidants studied are as follows: Cpd I(SH) (**A**), Cpd I(OH) (**B**), Cpd I(Cl) (**C**), Cpd I(ImP) (**D**), Cpd I(C*c*P) (**E**), Fe^{IV}═O(TMCS)$^+$ (**F**), and Cpd I(TauD) (**G**).

Correlation of Barrier Height with Polarizability. In the past we showed that atomization enthalpies of analogous molecules are linearly related with the difference in polarizability volume ($\Delta\alpha_{AV}$) for atomization,[45] whereby this polarizability difference was defined as the polarizability of molecule *M* (α_M) minus the sum of the atomic polarizabilities of its contents (α_{atoms}), eq 4.

$$\Delta\alpha_{AV} = \alpha_M - \sum \alpha_{atoms} \qquad (4)$$

To test whether the barrier height of substrate epoxidation reactions follows a similar correlation with polarizability volume, we took the polarizability trace from the Gaussian frequency calculations and estimated the polarizability difference for the process from reactants to transition state geometry. The polarizability difference ($\Delta\alpha_{AV}$) is calculated as the difference in polarizability trace between that for the transition state (α_{TS}) with respect to that for isolated reactants, i.e. Cpd I and substrate (Sub) as follows:

(45) de Visser, S. P. *Phys. Chem. Chem. Phys.* **1999**, *1*, 749–753.

$$\Delta\alpha_{AV} = \alpha_{TS} - \alpha_{CpdI} - \alpha_{Sub} \quad (5)$$

A plot of the polarizability difference against barrier height of substrate epoxidation by Cpd I(SH) using the data from Table 1 is given in Figure 11. The correlation is reasonable and implicates the polarizability volume change as indeed being proportional to the energy change during the reaction. This change is the largest for systems with small reaction barriers. Therefore, the charge distribution in the transition state will influence the polarizability volume, and the more dramatic the change encountered is the lower the barrier heights will be.

Nature of the Ring-Closure Barrier. So far, this work was focused only on the rate determining C−O bond formation step. However, in two-state reactivity the ring-closure step cannot be neglected. The reason for that is because in porphyrin ligated iron complexes Cpd I appears in close lying doublet and quartet spin states, whereby the initial C−O bond activation is on close lying spin state surfaces. However, as shown above in Figure 4, after the intermediate the doublet and quartet spin state surfaces bifurcate due to differences in electron transfer mechanisms. As a consequence, the low-spin surface gives retention of the stereochemistry, whereas on the high-spin surface the intermediate has a finite lifetime and may give rearrangement or side reactions.

The ring-closure barrier in all cases discussed in this work is small and generally much lower in energy than the C−O bond activation transition state. In addition, in several cases it was shown that no radical intermediate exists and the reaction collapses to products immediately. This has important consequences, since the lifetime of the radical intermediate may, for instance, lead to stereochemical scrambling and the formation of e.g. *cis*-epoxides from *trans*-olefins. In cases where no intermediate was found, the reaction will retain its stereochemical preference and no scrambling will occur. Figure 12 explains the ring-closure processes on the quartet and doublet spin state surfaces starting from the radical intermediates in the Fe(IV) electronic configuration, i.e. with orbital occupation $\delta_{x^2-y^2}{}^2\,\pi^*_{xz}{}^1\,\pi^*_{yz}{}^1\,a_{2u}{}^2\,\phi_{Sub}{}^1$. Thus, on the low-spin surface there is a radical on the terminal CH_2 group with a down-spin and an up-spin unpaired electron on the oxo group. These two electrons will pair up and form the C−O bond. Since these two electrons are already aligned in the intermediate complex, it will cost very little energy to close the bond, which is in agreement with the calculated potential energy surfaces. The promotion gap in the low-spin state is proportional to the IE of the substrate and the electron affinity of Cpd I.

In the high-spin state the situation is slightly different, whereby an electron has to transfer from the oxo group into a $\sigma^*_{z^2}$ orbital to create a product electronic configuration $\delta_{x^2-y^2}{}^2\,\pi^*_{xz}{}^1\,\pi^*_{yz}{}^1\,\sigma^*_{z^2}{}^1\,a_{2u}{}^2$. As a consequence, the promotion gap is larger in the high-spin ring closure than it is for the low-spin, and as a result also the ring-closure barrier is widened. Therefore, the high-spin surface is expected to proceed via a radical intermediate with a finite lifetime, while on the low-spin surface its lifetime is ultrashort and lead to products instantaneously. Consequently, the low-spin mechanism will retain its stereochemical preference, whereas stereochemical scrambling may occur on the high-spin surface, so that the two spin state surfaces are expected to lead to different product distributions. The epoxidation ring-closure mechanism follows similar electron transfer mechanisms to the rebound mechanism in aliphatic hydroxylation reactions, where also the doublet spin mechanism is barrierless or small, while the quartet spin rebound encounters significantly higher rebound barriers.[40]

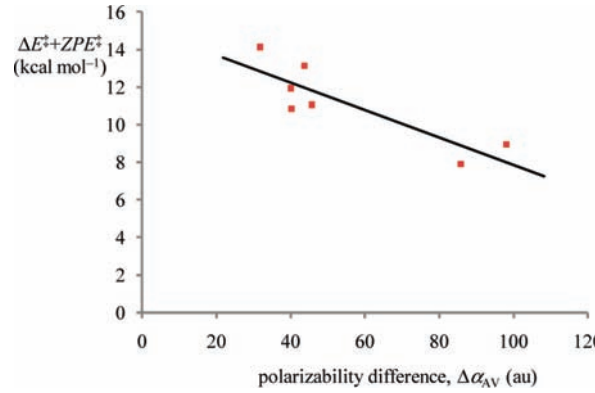

Figure 11. Correlation of epoxidation barrier height with polarizability difference for substrate epoxidation by Cpd I(SH).

In experimental work often stereochemical scrambling occurs, where *cis*-olefins give *trans*-epoxides, although the product ratios of *cis*- and *trans*-epoxides appear to be dependent on the reaction conditions and the nature of the oxidant.[46] For instance, experimental studies of *cis*-β-methylstyrene epoxidation using biomimetic iron porphyrins, such as Fe^{IV}═O($TMP^{+\bullet}$)L with L = F^-, Cl^-, or ClO_4^-, found retention of the stereochemistry when the experiment was performed at 0 °C or room temperature (>96% *cis*-epoxide products), whereas at lower temperatures (−78 °C) the *trans*-epoxide products were dominant.[18d] These studies support our general mechanism shown in Figures 5 and 12 that predict the intermediate complex to be in a shallow minimum that is separated from products by a small ring-closure barrier. At lower temperatures, the lifetime of the intermediate complex will be longer during which an internal rotation within the radical intermediate can take place that leads to stereochemical scrambling and the conversion of *cis*-olefins into *trans*-epoxides.

In addition, the studies of Gross et al.[18d] suggested that with strong electron-withdrawing axial ligands the radical intermediate has the Fe^{IV}(Por)OCH_2CHR conformation, whereas with weaker axial ligands the Fe^{III}($Por^{+\bullet}$)OCH_2CHR conformation is the lowest in energy. Indeed, in the case of propene epoxidation by Cpd I(CcP) the lowest lying C−O activation barrier is of the Fe^{III}-form, with the Fe^{IV} state 1.1 kcal mol^{-1} higher in energy.[47] Previous studies showed the difference between these two states to be close in energy for Cpd I(SH),[35] and environmental perturbations, such as solvent, influence their state ordering.

Other experimental studies showed that the nature of the olefin determined the rate constants for a set of olefin epoxidation studies by a biomimetic iron−porphyrin system.[48] This observation is in agreement with our correlation shown above between barrier height and ionization energy.

Differences and Comparisons between Substrate Epoxidation and Hydroxylation by Iron(IV)-Oxo Oxidants. So what are the fundamental differences between substrate epoxidation and substrate hydroxylation? First, as shown above the rate constant,

(46) Collman, J. P.; Brauman, J. I.; Meunier, B.; Hayashi, T.; Kodadek, T.; Raybuck, S. A. *J. Am. Chem. Soc.* **1985**, *107*, 2000–2005.
(47) de Visser, S. P. The axial ligand effect on substrate monoxygenation by the oxo-iron active species of heme enzymes. How does cytochrome c peroxidase compare to cytochrome P450? In *Inorganic Biochemistry: Research Progress*; Hughes, J. G., Robinson, A. J., Eds.; Nova Science Publishers, Inc.: New York, 2008; Chapter 7, pp 197−224.
(48) Collman, J. P.; Kodadek, T.; Raybuck, S. A.; Brauman, J. I.; Papazian, L. M. *J. Am. Chem. Soc.* **1985**, *107*, 4343–4345.

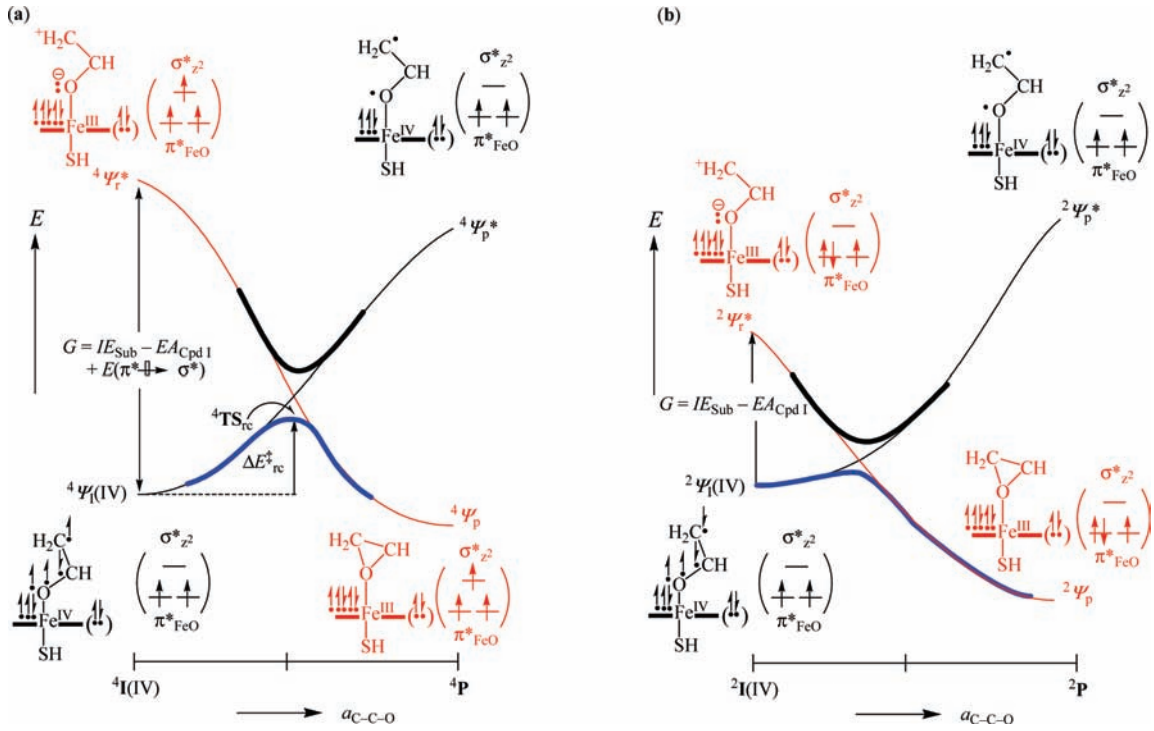

Figure 12. VB curve crossing diagram for high-spin and low-spin ring-closure mechanisms starting from ^{4,2}**I**(Fe^{IV}).

and hence the free energy of activation, of an epoxidation reaction correlates with the IE of the substrate as well as with the BDE_{OH} value of the iron-hydroxo complex and the polarizability change for the reaction. By contrast, a substrate hydroxylation has a rate-determining hydrogen atom abstraction whereby the barrier is related to BDE_{CH} and BDE_{OH}.[20,21,26] Since, aliphatic hydroxylation and double bond epoxidation both correlate with BDE_{OH}, this implies that the regioselectivity of aliphatic hydroxylation versus epoxidation is determined by the difference in IE of the substrate and the strength of the C−H bond of the substrate *but not by the intrinsic properties of the oxidant*. Propene epoxidation and aliphatic hydroxylation were studied with DFT using all oxidants shown in Figure 3, which enables us to calculate the ratio of epoxidation versus hydrogen atom abstraction barriers for a selection of different oxidants. Thus an average ratio of hydrogen atom abstraction over double bond epoxidation of $\mathbf{TS}_H/\mathbf{TS}_E = 1.17 \pm 0.17$ was found, with generally a preference of substrate hydroxylation over double bond epoxidation in the gas phase. Within the error of the calculations this ratio supports our observation that the nature of the oxidant does not affect the regioselectivity of substrate hydroxylation over epoxidation. This hydroxylation/epoxidation product ratio is in excellent agreement with that found by Vaz et al.[15] for cyclohexene epoxidation by P450 Δ2B4 and Δ2E1 isozymes. Moreover, the free energy of activation for styrene epoxidation[25a] by Cpd I(SH) calculated at 298 K is within 3 kcal mol^{-1} of the experimentally determined value of Vaz et al. More recent studies of the Newcomb group[14d] of styrene epoxidation and benzyl alcohol hydroxylation by CYP119 and CYP102HD isozymes showed similar kinetics and thermodynamics for each substrate, hence supporting our hypothesis that the regioselectivity of substrate hydroxylation versus epoxidation is dependent on the substrate only.

It should be realized, however, that BDE_{CH} is essentially the sum of an electron and a proton transfer. Nevertheless, the electron and proton transfers usually happen simultaneously so that the BDE_{CH} cannot be split into separate electron and proton transfer mechanisms. Therefore, the regioselectivity of substrate epoxidation versus hydroxylation is determined by the IE of the substrate relative to the BDE_{CH} value.

Conclusions

In this study we delineate the fundamental factors responsible for substrate epoxidation by an iron(IV)-oxo heme and nonheme systems through computational and VB methods. Substrate epoxidation by the iron(IV)-oxo system depends on the IE of the substrate and not on the oxidants. We show that the reactions are stepwise via a radical intermediate. The rate -determining step is the initial C−O bond formation transition state, which is found to correlate with the ionization energy of the substrate, the BDE_{OH} of the oxidant, and the polarizability change for the reaction. These properties are explained with a VB curve crossing diagram that identifies the electron transfer mechanisms in the process. It is further shown that the regioselectivity of substrate epoxidation versus hydroxylation is not dependent on the choice of the oxidant, but the thermodynamics of the reaction is.

Acknowledgment. The research was supported by CPU time provided by the National Service of Computational Chemistry Software (NSCCS). D.K. is the Ramanujan Fellow of the Department of Science and Technology (New Delhi). Prof Sason Shaik is acknowledged for helpful discussions regarding the Valence Bond diagram and critical proofreading of our manuscript.

Supporting Information Available: Cartesian coordinates of all structures, tables with group spin densities, charges and absolute energies of all structures calculated in this work. Also given are seven figures with correlations of geometric parameters with barrier height as well as complete ref 23. This material is available free of charge via the Internet at http://pubs.acs.org.

JA9106176